American Mineralogist, Volume 59, pages 98–109, 1974

The Diopside-Orthoenstatite Two-Phase Region in the System $CaMgSi_2O_6$–$Mg_2Si_2O_6$

RICHARD D. WARNER[1], AND WILLIAM C. LUTH

Department of Geology, Stanford University, Stanford, California 94305

Abstract

The solvi bounding the diopside-orthoenstatite two-phase region in the system $CaMgSi_2O_6$–$Mg_2Si_2O_6$ are determined over the temperature range 900°–1300°C at 2, 5, and 10 kbar. An obvious break along the diopside limb occurs above 1100°C at 2 kbar, and is attributed to either (1) non-equilibrium of runs below 1100°C, or (2) a narrow region of two-phase unmixing. Detailed X-ray study with a focussing Guinier-de Wolff camera, supplemented by electron probe microanalyses, fail to provide a definitive resolution of this problem. The experimental data above 1100°C are analyzed in terms of least-squares fitting to a two-constant (W_{G1}, W_{G2}) Margules equation (Thompson, 1967) in order to derive analytic expressions for the solvus boundary. The simplest, best representation of the data is given by the equations

$$W_{G1} = 12,189 \pm 864 - 2,419 \pm 581 \times T(°K)/1000 + 36.6 \pm 10.4 \times P(kbar),\ s_y = 204.5$$

$$W_{G2} = 24,032 \pm 1,697 - 12,215 \pm 1,153 \times T(°K)/1000,\ s_y = 408.9$$

A 30 kbar solvus calculated from these equations is in good agreement with the 30 kbar solvus determined experimentally by Davis and Boyd (1966).

The amount of $Mg_2Si_2O_6$ dissolved in diopside may be used to estimate temperatures of equilibration for mineral assemblages characterized by the coexistence of diopsidic clinopyroxene and enstatitic orthopyroxene. Application to coexisting pyroxenes from peridotite nodules in kimberlites (analyses reported by Davis and Boyd, 1966; Boyd, 1969, 1970b) gives two populations of equilibration temperatures for these assemblages, with cluster points near 1025°C (calcic diopsides) and 1350°C (subcalcic diopsides).

Introduction

The join $CaMgSi_2O_6$–$Mg_2Si_2O_6$ is one of the more important "simple" systems relevant to the petrogenesis of mafic and ultramafic rocks. Subsolidus equilibria in this system are governed by partial immiscibility between the Ca-rich and Ca-poor end-member phases (Atlas, 1952; Boyd and Schairer, 1964; Davis and Boyd, 1966). Polymorphism in the Ca-poor region of the join considerably complicates the subsolidus phase relations (Atlas, 1952; Boyd and Schairer, 1964; Kushiro, 1969; Smith, 1969).

Principal emphasis in the present study is directed toward delimitation of the diopside-orthoenstatite two-phase region as a function of temperature and pressure. The complications introduced because of polymorphism are of concern here only insofar as the stability interval of the diopside-orthoenstatite two-phase coexistence is affected. Through numerical analysis of the experimental data, an analytic representation for the solvus bounding the two-phase region may be obtained (Thompson and Waldbaum, 1969; Luth and Fenn, 1973). Such a representation may permit extrapolation of the boundary to conditions of pressure and temperature beyond the range of experimental observation. The results may be applied to natural assemblages containing coexisting Ca-rich clinopyroxene and Ca-poor orthopyroxene phases in order to obtain estimates of equilibration temperatures, provided the compositions involved correspond to the binary system $CaMgSi_2O_6$–$Mg_2Si_2O_6$.

Previous Work

Atlas (1952) studied subsolidus equilibria along the join $CaMgSi_2O_6$–$Mg_2Si_2O_6$ at 1 bar and demonstrated that the dominant feature is the existence of a region of immiscibility separating the fields of Ca-rich and Ca-poor pyroxene. According to Atlas's results, the solvus does not intersect the solidus, but crests at a temperature (about 1375°C) slightly below the solidus. From his study of the polymorphism of

[1] Present Address: Planetology Branch, Code 644, Goddard Space Flight Center, Greenbelt, Maryland 20771

$MgSiO_3$, Atlas suggested that orthoenstatite coexists with diopside at temperatures up to 1100°C; this is succeeded at higher temperatures by the two-phase coexistences, namely, protoenstatite-diopside (1100° C < T < 1250°C) and clinoenstatite-diopside (T > 1250°C).

Boyd and Schairer (1964) further studied this join at 1 bar and, hydrothermally, at pressures up to 1000 bars. Their results indicated less extensive crystalline solution than Atlas's determinations, and showed that the solvus intersects the solidus over a composition interval of nearly 35 mole percent. Again, the upper limit of the diopside-orthoenstatite coexistence at 1 bar was found to be 1100°C.

Davis and Boyd (1966) mapped the diopside-orthoenstatite two-phase region at a pressure of 30 kbar and encountered no polymorphic inversions to solidus temperatures. Kushiro (1969) has since shown that their results above 1400°C are probably incorrect, inasmuch as he has demonstrated a high temperature stability field for "iron-free" pigeonite on the $CaMgSi_2O_6$–$Mg_2Si_2O_6$ join at 20 kbar. The appearance of a high-temperature pigeonite field imposes an upper limit on the diopside-orthoenstatite two-phase region. Kushiro and Yoder (1970) investigated the lower stability limit of iron-free pigeonite and suggested that its stability field extends to low pressures, possibly even to 1 bar. Warner (1971), Yang and Foster (1972), and Kushiro (1972) have independently concluded that pigeonite is stable on the join $CaMgSi_2O_6$–$Mg_2Si_2O_6$ at 1 bar. Presumably this phase is equivalent to that designated as clinoenstatite solid solution by Atlas (1952).

Experimental Results

Starting materials

Compositions at intervals of 5 wt percent along the join $CaMgSi_2O_6$–$Mg_2Si_2O_6$ were prepared as mechanical mixtures of crystalline diopside and clinoenstatite, which had previously been synthesized from the oxides (method described in Warner and Luth, 1973). Also prepared in this manner were compositions along the joins $CaMgSi_2O_6$–SiO_2, $CaMgSi_2O_6$–Mg_2SiO_4, $CaMgSi_2O_6$–$CaMgSiO_4$, $CaMgSi_2O_6$–$Mg_2Si_2O_6$ + 5 wt percent SiO_2, and $CaMgSi_2O_6$–$Mg_2Si_2O_6$ + 5 wt percent Mg_2SiO_4. In addition to these mechanical mixtures of crystalline end-member phases, a series of homogeneous glass compositions, which had been made by Dr. J. F. Schairer at the Geophysical Laboratory and given to one of us (WCL), were also used for starting materials, but only in a small number of experiments (appropriately indicated in our run tables).

Unit cell dimensions of synthetic pyroxenes

Synthesis of single-phase pyroxenes along the join $CaMgSi_2O_6$–$Mg_2Si_2O_6$ (apparatus and experimental procedure described in Warner and Luth, 1973) was undertaken for the primary purpose of establishing X-ray determinative curves for rapid measurement of pyroxene compositions (Fig. 2). Conditions of synthesis and the resultant phase products are given in Table 1. Microscopic examination of the run products, using oil immersion grain mounts, was supplemented by X-ray powder diffraction analysis with a focussing camera (Nonius Guinier-de Wolff) set for Cu$K\alpha$ radiation. Spinel (U.S. Bureau of Mines, Norris, Tennessee; a = 8.0833 Å at 25°C) was used as an internal standard. Unit cell dimensions for single-phase pyroxenes were derived through the use of a least squares cell refinement computer program developed by Evans, Appleman, and Handwerker (1963), and modified to run on an IBM 360/67 computer. Results of least squares cell refinements are given in Table 2. As expected, substitution of Mg for Ca results in a fairly regular decrease in a, b, c, and unit cell volume, with the effect being largest for a and smallest for c. The β angle for diopsidic ($C2/c$) pyroxenes increases substantially with Mg for Ca substitution.

Unit cell refinements for a series of clinopyroxenes ($di_{20}en_{80}$–di_5en_{95})[2] synthesized at 1350°C and 1 bar produced a marked hiatus in cell parameters between $di_{10}en_{90}$ and di_5en_{95}. Close examination of the X-ray film patterns for $di_{10}en_{90}$ and di_5en_{95} revealed splitting of the 002 and $\bar{2}02$ peaks, and weak protoenstatite lines were discerned. Although the entire series of runs was made in the field labeled Pr_{ss} by Boyd and Schairer (1964, Fig. 1), the interpretation was made (Warner, 1971, p. 99) that a field of $P2_1/c$ clinopyroxene is stable on the join $CaMgSi_2O_6$–$Mg_2Si_2O_6$ at 1 bar, and that this field is separated from the (more Mg-rich) Pr_{ss} field by a narrow two-phase region (Warner, 1971, Fig. 15a). This interpretation is consistent with the polymorphic relations originally deduced by Atlas (1952), and with the high pressure results obtained by Kushiro (1969), if it is assumed that the stability field for "iron-free" pigeonite extends to 1 bar. Kushiro (1972) and Yang and Foster

[2] di_xen_y, composition given in wt percent.

TABLE 1. Pyroxene Synthesis Data

Starting material[#] composition	T(°C)	t(hrs)	Results[##]
a) 1 bar data			
*di_{100} (glass)	1350	24	Di
*$di_{95}en_5$	1350	108	Di_{ss}
*$di_{90}en_{10}$	"	"	Di_{ss}
*$di_{85}en_{15}$	"	"	Di_{ss}
*$di_{80}en_{20}$	1350	121	Di_{ss}
$di_{75}en_{25}$	"	"	Di_{ss}+$\underline{Pig}_{ss}$
$di_{70}en_{30}$	"	"	Di_{ss}+$\underline{Pig}_{ss}$
*$di_{20}en_{80}$	1350	156	Pig_{ss}+$\underline{Cr}$'
*$di_{15}en_{85}$	"	"	Pig_{ss}+$\underline{Cr}$'
$di_{10}en_{90}$	"	"	Pig_{ss}+$\underline{Pr}_{ss}$+$\underline{Cr}$'
di_5en_{95}	"	"	Pig_{ss}+$\underline{Pr}_{ss}$+$\underline{Cr}$'
$di_{96}q_4$ (glass)	1350	168	Di_{ss}+L
$di_{95}en_5$ + 5 wt. % q	"	"	Di_{ss}+L+$\underline{Cr}$'
$di_{85}en_{10}q_5$ (glass)	"	"	Di_{ss}+Cr'
$di_{80}en_{15}q_5$ (glass)	"	"	Di_{ss}+Cr'
$di_{75}en_{20}q_5$ (glass)	"	"	Di_{ss}+Cr'
$di_{95}en_5$ + 5 wt. % fo	1350	168	Di_{ss}+$\underline{Fo}_{ss}$
$di_{90}en_{10}$ + 5 wt. % fo	"	"	Di_{ss}+$\underline{Fo}_{ss}$
$di_{85}en_{15}$ + 5 wt. % fo	"	"	Di_{ss}+$\underline{Fo}_{ss}$
$di_{75}en_{25}$ + 5 wt. % fo	"	"	Di_{ss}+$\underline{Pig}_{ss}$+$\underline{Fo}_{ss}$
*$di_{95}mo_5$	1350	168	Di_{ss}
$di_{90}mo_{10}$	"	"	Di_{ss}+$\underline{Ak}_{ss}$+$\underline{Fo}_{ss}$
*$di_{95}fo_5$	"	"	Di_{ss}
$di_{90}fo_{10}$	"	"	Di_{ss}+Fo_{ss}
*$di_{80}en_{20}$	1375	86	Di_{ss}
*$di_{75}en_{25}$	"	"	Di_{ss}
*$di_{70}en_{30}$	"	"	Di_{ss}
*$di_{90}en_{10}$ (Di_{ss})[1]	"	"	Di_{ss}
*$di_{85}en_{15}$ (Di_{ss})[1]	"	"	Di_{ss}
$di_{65}en_{35}$	1375	72	Di_{ss}+$\underline{Pig}_{ss}$
$di_{60}en_{40}$	"	"	Di_{ss}+$\underline{Pig}_{ss}$
*$di_{25}en_{75}$	"	"	Pig_{ss}
*$di_{20}en_{80}$	"	"	Pig_{ss}
*$di_{15}en_{85}$	"	"	Pig_{ss}

Starting material[#] composition	Wt. percent H_2O	P(bars)	T(°C)	t(hrs)	Results[##]
b) hydrothermal data					
*di_{100}	2.5	1000	1280	21	Di_{ss}+$\underline{L}$
*$di_{95}en_5$	2.3	"	"	"	Di_{ss}+$\underline{L}$
*$di_{90}en_{10}$	4.4	"	"	"	Di_{ss}+$\underline{L}$
*$di_{85}en_{15}$	2.6	"	"	"	Di_{ss}+$\underline{L}$
*$di_{80}en_{20}$	2.9	"	"	"	Di_{ss}+$\underline{L}$
*$di_{75}en_{25}$	2.7	"	"	"	Di_{ss}+$\underline{L}$
$di_{95}en_5$	3.0	2000	1150	72	Di_{ss}+V
$di_{92.5}en_{7.5}$	5.0	"	"	"	Di_{ss}+V
$di_{90}en_{10}$	5.8	"	"	"	Di_{ss}+V
$di_{87.5}en_{12.5}$	5.2	"	"	"	Di_{ss}+V
$di_{85}en_{15}$	4.5	"	"	"	Di_{ss}+$\underline{En}_{ss}$+V
$di_{82.5}en_{17.5}$	6.0	"	"	"	Di_{ss}+$\underline{En}_{ss}$+V
$di_{80}en_{20}$	10	"	"	"	Di_{ss}+$\underline{En}_{ss}$+V
$di_{15}en_{85}$	18	2000	1150	86	En_{ss}+Di_{ss}+V
$di_{10}en_{90}$	20	"	"	"	En_{ss}+$\underline{Di}_{ss}$+V
di_5en_{95}	20	"	"	"	En_{ss}+Cen_{ss}+V
$di_{90}en_{10}$ (Di_{ss})[2]	12.2	2000	1200	17	Di_{ss}+V
$di_{85}en_{15}$ (Di_{ss})[2]	9.5	"	"	"	Di_{ss}+V
$di_{85}en_{10}q_5$ (glass)	12.9	"	"	"	Di_{ss}+$\underline{L}$+V
*en_{100}	19	5000	1000	91	En+V
$di_{15}en_{85}$	20	5000	1200	32	En_{ss}+Di_{ss}+$\underline{Fo}_{ss}$+V
$di_{10}en_{90}$	18	"	"	"	En_{ss}+$\underline{Di}_{ss}$+V
*di_5en_{95}	17	"	"	"	En_{ss}+V
$di_{95}en_5$	20	5000	1250	24	Di_{ss}+V
*$di_{90}en_{10}$	20	"	"	"	Di_{ss}+$\underline{L}$+V
*$di_{85}en_{15}$	20	"	"	"	Di_{ss}+$\underline{Fo}_{ss}$+$\underline{L}$+V
$di_{80}en_{20}$	20	"	"	"	Di_{ss}+$\underline{Fo}_{ss}$+$\underline{L}$+V
*en_{100}	13	10,000	1000	70	En+V
*di_{100}	13	10,000	1050	67	Di_{ss}+V
*$di_{2.5}en_{97.5}$	18	"	"	"	En_{ss}+V
*$di_{85}en_{15}$	33	10,000	1100	24	Di_{ss}+$\underline{Fo}_{ss}$+V
*$di_{85}en_{15}$	25	"	"	"	Di_{ss}+$\underline{Fo}_{ss}$+V
*$di_{85}en_{15}$	14.5	"	"	"	Di_{ss}+$\underline{Fo}_{ss}$+V
*$di_{85}en_{15}$	4.8	"	"	"	Di_{ss}+V
*$di_{90}en_{10}$ (Di_{ss})[2]	18	"	"	"	Di_{ss}+V
*$di_{85}en_{15}$ (Di_{ss})[2]	19.5	"	"	"	Di_{ss}+V

[#]Unless otherwise noted, starting material used was a mechanical mixture of the crystalline end-member phases. Component designations: di = $CaMgSi_2O_6$; en = $Mg_2Si_2O_6$; q = SiO_2; fo = Mg_2SiO_4; mo = $CaMgSiO_4$

[##]Phase designations: Di = diopside; En = orthoenstatite; Cen = clinoenstatite; Pr = protoenstatite; Pig = pigeonite; Cr = cristobalite; Fo = forsterite; Ak = akermanite; L = silicate liquid; V = hydrous vapor. Other designations: ss = solid solution; _ = amount of phase present estimated at less than 5 volume percent; ' = presence of phase thought to be metastable.

* = least squares cell refinement performed on pyroxene (Table 2)

[1]Di_{ss} synthesized hydrothermally at 1250°C and 5 kbar

[2]Di_{ss} synthesized at 1350°C and 1 bar

(1972) have independently confirmed the phase relations suggested by Warner (1971). The range of stable pigeonite crystalline solutions encompasses the approximate composition interval $di_{25}en_{75}$–$di_{15}en_{85}$ at 1375°C and 1 bar. Unit cell dimensions for synthetic iron-free pigeonite are given in Table 2d.

A series of hydrothermal syntheses at 1200°C and 5 kbar, spanning the composition range $di_{95}en_5$–$di_{80}en_{20}$, yielded what are considered to be anomalously large cell dimensions for the respective diopside crystalline solutions. Trace amounts of forsterite were detected in some of the products, which suggests that the bulk crystalline assemblages lie in the region $CaMgSi_2O_6$–$Mg_2Si_2O_6$–Mg_2SiO_4. The presence

of small amounts of forsterite in hydrothermal crystallizations of the composition $MgSiO_3$ has previously been noted by Kushiro, Yoder, and Nishikawa (1968); they concluded that the vapor phase had a higher proportion of SiO_2:MgO than the pyroxene. In order to ascertain whether the anomalous cell dimensions are the result of silica-leaching by the vapor phase, the following experiments were performed.

(i) A series of syntheses were made at 1190°C and 10 kbar, using the anhydrous composition $di_{85}en_{15}$ and varying the water content of the samples. A regular increase in the unit cell dimensions is observed with increasing water content (Table 2b), and there is a corresponding increase in the amount of forsterite present. No forsterite was detected in the sample which contained only 4.8 wt percent H_2O. The results are schematically illustrated in Figure 1, where (V) is a hypothetical composition for the solid silicate material dissolved in the water-rich vapor phase. The effect of vapor-phase leaching is to drive the crystalline assemblages across Di_{ss}–Fo_{ss} tie lines, thus producing a more diopside-rich pyroxene (*i.e.*, a pyroxene with larger cell dimensions). It is apparent that the observed shift in cell dimensions can be satisfactorily accounted for by supposing a high proportion of silica in the vapor phase.

(ii) Two of the compositions that were hydrothermally synthesized at 1200°C, 5 kbar (N_{en} = 0.107, 20 wt percent H_2O; N_{en} = 0.160, 20 wt percent H_2O) were rerun at 1350° and 1 bar. In both cases, measurable decreases in the cell parameters were observed (for example, from 439.21 to 438.52 Å^3, and 438.62 to 437.79 Å^3, respectively, for unit cell

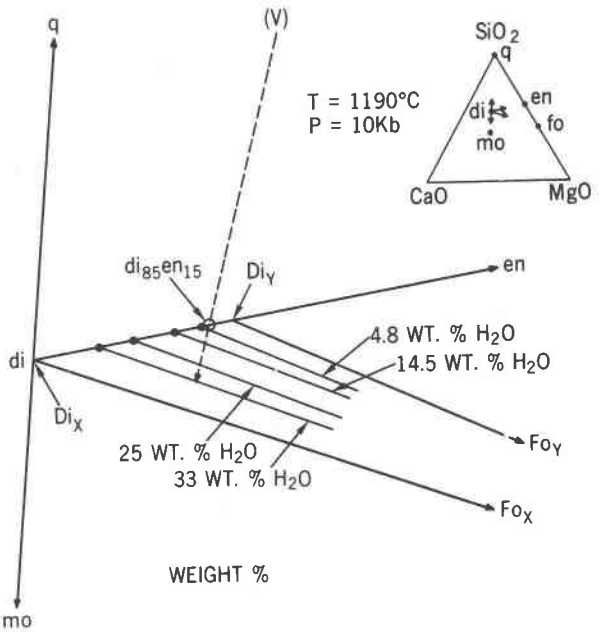

FIG. 1. Schematic interpretation of results for runs with variable wt percent H_2O at 1190°C and 10 kbar. Closed circles represent composition of Di_{ss} (coexisting with Fo_{ss} and vapor) as determined from $2\theta_{112}$ (Fig. 2). The observed variation in unit cell parameters with increased H_2O content for the anhydrous composition $di_{85}en_{15}$ can be accounted for by supposing that the composition, V, of the silicate material dissolved in the water-rich vapor phase is significantly more silica-rich than $di_{85}en_{15}$. With increasing H_2O content, the bulk crystalline composition is driven across Di_{ss}–Fo_{ss} tie lines toward the limiting Di_x–Fo_x tie line of the Di_{ss} + Fo_{ss} + V three-phase volume (Di_y–Fo_y is the other limiting tie line of this volume). Phase and component designations as in Table 1.

TABLE 2. Unit Cell Dimensions of Synthetic Pyroxenes

Wt. % H_2O	N_{en}	a(Å)	b(Å)	c(Å)	β(°)	V(Å^3)	n/m
		a) Diopside crystalline solutions					
0	0.000	9.7506(8)	8.9294(7)	5.2518(4)	105 53.9(4)	439.76(4)	32/33
2.5	"	9.7501(10)	8.9288(9)	5.2507(5)	105 52.7(5)	439.67(5)	32/32
18	"	9.7498(20)	8.9283(13)	5.2535(6)	105 49.6(9)	439.98(9)	19/20
0	0.054	9.7469(12)	8.9303(11)	5.2512(6)	105 58.3(6)	439.43(6)	32/32
2.3	"	9.7468(14)	8.9280(11)	5.2504(5)	105 56.8(6)	439.31(6)	28/28
0	0.107	9.7428(9)	8.9266(8)	5.2504(5)	106 06.8(5)	438.69(5)	27/27
4.4	"	9.7464(12)	8.9258(10)	5.2497(5)	106 05.6(5)	438.80(6)	28/28
0	0.160	9.7381(13)	8.9232(10)	5.2495(6)	106 15.9(6)	437.90(6)	32/32
2.6	"	9.7373(7)	8.9211(6)	5.2477(3)	106 14.7(4)	437.65(4)	31/31
0	0.212	9.7351(15)	8.9202(11)	5.2490(7)	106 28.9(8)	437.09(8)	22/23
0	"	9.7364(18)	8.9198(12)	5.2470(7)	106 23.2(1.0)	437.17(8)	25/25
2.9	"	9.7371(11)	8.9217(10)	5.2473(6)	106 22.5(6)	437.34(6)	30/30
0	0.264	9.7286(20)	8.9138(13)	5.2456(7)	106 32.3(1.0)	436.08(9)	25/25
2.7	"	9.7318(13)	8.9140(8)	5.2469(5)	106 30.4(7)	436.40(6)	23/23
0	0.316	9.7273(23)	8.9099(11)	5.2460(7)	106 45.2(1.1)	435.36(9)	20/22
		b) Runs with variable wt. percent H_2O					
18	0.107	9.7477(20)	8.9287(15)	5.2506(7)	106 00.7(1.0)	439.25(9)	19/19
20	"	9.7469(14)	8.9264(12)	5.2522(6)	106 01.5(7)	439.21(7)	25/25
0	"	9.7424(14)	8.9240(11)	5.2484(5)	106 03.0(7)	438.52(7)	20/20
19.5	0.160	9.7445(16)	8.9230(12)	5.2491(5)	106 05.2(7)	438.54(7)	22/22
20	"	9.7442(9)	8.9254(9)	5.2506(4)	106 09.5(5)	438.62(5)	26/26
0	"	9.7371(30)	8.9225(16)	5.2490(9)	106 15.3(1.7)	437.79(14)	16/16
33	0.160	9.7487(8)	8.9278(6)	5.2507(3)	106 00.1(3)	439.29(4)	23/23
25	"	9.7434(8)	8.9267(7)	5.2491(3)	106 02.6(3)	438.77(4)	27/28
14.5	"	9.7413(12)	8.9235(6)	5.2484(4)	106 10.3(5)	438.17(5)	23/23
4.8	"	9.7388(8)	8.9228(6)	5.2479(3)	106 13.9(4)	437.85(4)	25/25
		c) Ternary diopside crystalline solutions					
0	$di_{95}mo_5$	9.7522(9)	8.9276(9)	5.2525(4)	105 52.4(4)	439.87(5)	28/28
0	$di_{95}fo_5$	9.7499(8)	8.9250(7)	5.2509(4)	105 57.7(4)	439.31(4)	29/29
		d) Pigeonite crystalline solutions					
0	0.764	9.6679(30)	8.8572(16)	5.2145(7)	108 20.9(1.3)	423.82(12)	18/20
0	0.812	9.6600(22)	8.8513(9)	5.2075(5)	108 20.7(8)	422.63(8)	22/28
0	"	9.6602(13)	8.8508(7)	5.2086(5)	108 21.2(6)	422.69(6)	25/32
0	0.859	9.6475(21)	8.8456(11)	5.1999(5)	108 23.2(9)	421.10(8)	16/20
0	"	9.6528(15)	8.8452(9)	5.2030(5)	108 22.4(7)	421.59(7)	22/28
		e) Orthoenstatite crystalline solutions					
17	0.953	18.2483(32)	8.8306(15)	5.1889(8)		836.15(17)	22/27
18	0.977	18.2427(33)	8.8277(27)	5.1848(9)		834.97(22)	21/23
19	1.000	18.2180(33)	8.8159(20)	5.1784(7)		831.68(18)	19/23
13	"	18.2296(19)	8.8192(9)	5.1777(4)		832.43(10)	33/40

n/m = number of lines used in refinement/number of input diffraction lines

Numbers in () represent errors in final figures at the unit weight standard error level

volume). Also, two compositions previously synthesized at 1350°C, 1 bar, were rerun at 1190°C, 10 kbar (N_{en} = 0.107, 18 wt percent H_2O; N_{en} = 0.160, 19.5 wt percent H_2O). Here, the cell volumes were found to increase proportionately (from 438.69 to 439.25 Å^3, and 437.90 to 438.54 Å^3, respectively). These results are also consistent with the vapor-phase-leaching hypothesis.

The possibility of non-stoichiometry of diopside crystalline solutions, as discovered at 1 bar by Kushiro (1972), must also be entertained. By electron probe analysis of synthetic crystals, Kushiro (1972) showed that at near liquidus temperatures pyroxenes of the $CaMgSi_2O_6$–$MgSiO_3$ series that are slightly deficient in SiO_2 crystallize. However, crystalline solution up to 5 wt percent toward $CaMgSiO_4$ and Mg_2SiO_4 does not greatly change the unit cell parameters of diopside (Table 2c). Thus, although limited ($\ll$ 5 wt percent) non-stoichiometry toward the SiO_2-deficient region is a possible factor at 1200°C and 5 kbar, it is unlikely to cause the observed magnitude of shift in cell dimensions.

Results of two-phase determinations

The solvi bounding the diopside-orthoenstatite two-phase region were mapped as a function of temperature at 2, 5, and 10 kbar. The starting materials used were mechanical mixtures of diopside and clinoenstatite which had been previously synthesized from the oxides. However, the bulk compositions used lay well within the two-phase region (*i.e.*, $di_{60}en_{40}$–$di_{40}en_{60}$). In this manner, the solvus boundary was approached from outside the two-phase region (*i.e.*, by homogenization). To enhance equilibration, all experiments were carried out under hydrothermal conditions.

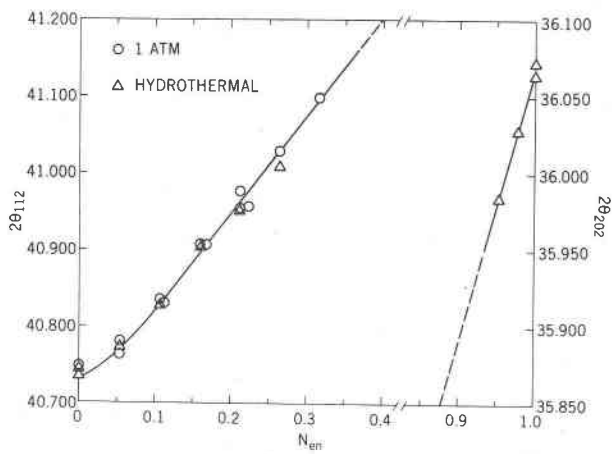

FIG. 2. The observed variation with N_{en} of $2\theta_{112}$ (diopside crystalline solution) and $2\theta_{202}$ (orthoenstatite crystalline solution) for Cu$K\alpha$ radiation. Symbols: open circles, 1 atm syntheses; open triangles, hydrothermal syntheses.

X-ray films of the run products were taken with a Nonius Guinier-de Wolff focussing powder camera using spinel (a = 8.0833 Å at 25°C) as an internal standard. Diopside compositions were then obtained by measuring $2\theta_{112}$; compositions of orthoenstatites were determined by measuring $2\theta_{202}$. The observed variation with mole fraction $Mg_2Si_2O_6$ (N_{en}) for these peaks is indicated in Figure 2. The diopside determinative curve flattens in the range $0 < N_{en} < 0.05$; all other compositional parameters appear to behave similarly (*cf* Boyd and Schairer, 1964). The compositional range over which the 112 peak can be used is restricted to between $0 < N_{en} < 0.40$ because of interference from the 022 peak of diopside at the more $Mg_2Si_2O_6$-rich compositions. This did not prove a problem in the P, T range studied. The estimated precision obtained through use of the curves in Figure 2 is about ± 0.015 N_{en} for orthoenstatite determinations, and ± 0.02 N_{en} for diopside determinations, except for the range $0 < N_{en} < 0.05$, where the estimated precision is about ± 0.03 N_{en}.

Homogenization experiments were carried out at approximately 50°C intervals from 800°–1300°C at 2, 5, and 10 kbar. In the temperature range 900°–1300°C, orthoenstatite coexisted with diopside at each isobar studied. At temperatures below 900°C, clinoenstatite (800°C at 2 and at 5 kbar), or a mixture of clinoenstatite and orthoenstatite (850°C at 2 and at 5 kbar; 800°C at 10 kbar), was found to coexist with diopside. Exceptions to this occurred in two runs at 850°C, 2 kbar and two at 850°C, 10 kbar, where orthoenstatite was the only polymorphic form of Ca-poor pyroxene present. The non-conversion or only partial conversion of clinoenstatite to orthoenstatite encountered in some of these results is attributed to sluggish reaction rates at these lower temperatures.

Atlas (1952) and Boyd and Schairer (1964) placed the upper termination of the diopside-orthoenstatite two-phase region near 1100°C at 1 bar. This termination corresponds to the inversion of Mg-rich orthoenstatite, saturated with $CaMgSi_2O_6$, to protoenstatite, according to the reaction En_{ss} = Pr_{ss} + Di_{ss}. The stability of the diopside-orthoenstatite two-phase coexistence to a temperature of at least 1300°C at 2 kbar found in our study, requires

the above reaction to possess a very steep, positive dT/dP slope. Such a steep slope would be consistent with that determined for the orthoenstatite = protoenstatite inversion curve in the unary system, $MgSiO_3$ ($dT/dP = 84° \pm 10°C$/kbar, Boyd, Schairer, and Davis, 1964).

Our experimentally derived data for the diopside-orthoenstatite two-phase region are given in Table 3. Determinations involving starting compositions containing 5–10 wt percent excess silica are included in Table 3, since pyroxenes of the $CaMgSi_2O_6$–$Mg_2Si_2O_6$ series show no solution toward SiO_2 (Kushiro and Schairer, 1963; Kushiro, 1972). In Table 3 we have included only data in the temperature range 1150°–1300°C at 2 kbar and 1100°–1300°C at 5 and 10 kbar. We have found our experimental results from 900°–1100°C (all pressures) to be of questionable interpretation as regards the diopside limb of the solvi (see following section) and have consequently eliminated them from inclusion in Table 3. Table 3 therefore represents the complete input data for our subsequent numerical analysis.

TABLE 3. Diopside-Orthoenstatite Two-Phase Data

T(°C)	t(hrs)	$2\theta^A_{112}$	$2\theta^B_{202}$	N_{2A}	N_{2B}	r
		a) 2 kbar data (homogenization)				
1150	72	40.869	35.969	0.139	0.944	0.083
1150	86	40.897	35.949	0.160	0.933	0.093
1200	45	40.931	35.930	0.187	0.923	0.110
"	"	40.911	35.946	0.171	0.931	0.102
"	"	40.958	35.915	0.208	0.914	0.122
1235	20	40.943	35.923	0.196	0.919	0.115
1250	72	41.006	35.918	0.246	0.916	0.162
1300	17	41.157	35.892	0.365	0.902	0.267
		b) 2 kbar data (reversal)				
1200	17	40.941	35.915	0.195	0.914	0.109
"	"	40.954	35.930	0.205	0.923	0.128
"	"	40.962	35.908	0.211	0.910	0.121
"	"	40.953	35.918	0.204	0.916	0.120
		c) 5 kbar data				
1100	66	40.848	35.983	0.122	0.952	0.074
"	"	40.836	35.977	0.112	0.949	0.061
1155	36	40.871	35.967	0.140	0.943	0.083
"	"	40.874	35.968	0.142	0.944	0.086
1200	32	40.893	35.968	0.157	0.944	0.101
1240	22	41.072	35.924	0.298	0.919	0.217
"	"	41.046	35.930	0.277	0.922	0.199
1250	24	40.960	35.925	0.209	0.920	0.129
1300	18	41.128	35.896	0.341	0.904	0.245
		d) 10 kbar data				
1100	90	40.829	35.988	0.107	0.955	0.062
"	"	40.849	35.993	0.123	0.958	0.081
1105	62	40.835	35.980	0.112	0.950	0.062
1150	19	40.860	35.968	0.131	0.944	0.075
1150	35	40.840	35.986	0.116	0.954	0.070
"	"	40.855	35.970	0.127	0.945	0.072
1190	24	40.886	35.963	0.152	0.941	0.093
"	"	40.916	35.942	0.175	0.929	0.104
1230	19	40.999	35.930	0.240	0.923	0.163
1300	12	41.097	35.901	0.317	0.906	0.223
"	"	41.085	35.911	0.307	0.912	0.219
1300	16	41.111	35.877	0.328	0.893	0.221

$2\theta^A_{112}{}_{solution}$ = observed value of $2\theta_{112}$ (Cu K_α radiation) for diopside crystalline solution

$2\theta^B_{202}$ = observed value of $2\theta_{202}$ for orthoenstatite crystalline solution

N_{2A} = mole fraction $Mg_2Si_2O_6$ in diopside crystalline solution

N_{2B} = mole fraction $Mg_2Si_2O_6$ in orthoenstatite crystalline solution

$r = N_{2A} + N_{2B} - 1$

All starting material compositions used were mixtures of the crystalline end-member phases, with the exception of the solvus reversal runs (see text)

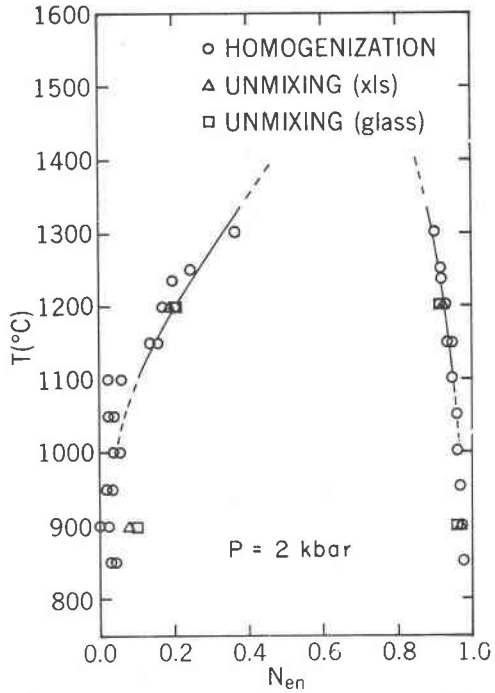

FIG. 3. Isobarbic, temperature-composition section of the diopside-orthoenstatite two-phase region at 2 kbar. The open circles indicate experimental determinations of the compositions of coexisting two-phase pairs. The solid curves represent boundaries for the two-phase region calculated from a two-constant (W_{G1}, W_{G2}) Margules equation, where $W_{G1} = A + BT + DP$ and $W_{G2} = A + BT$ (polynomial coefficients given in Table 5). Coexistence limits of the diopside + orthoenstatite assemblage are not shown, but the appearance of a stability field for pigeonite requires an upper temperature limit near 1330°C (Kushiro and Yoder, 1970, Fig. 18).

Reversals of the solvus boundary were attempted using (a) samples previously crystallized for a week at 1350°C and 1 bar, and (b) homogeneous glass compositions ($di_{60}en_{37.5}q_{2.5}$ and $di_{42}en_{54}q_4$) as starting materials. Very satisfactory reversals for both limbs were obtained at 1200°C, 2 kbar; at 900°C, 2 kbar, however, it was not possible to reverse the diopside limb, although the orthoenstatite limb proved reversible (Figure 3). Again, this indicates probable non-equilibrium in our lower temperature runs which have thus been excluded from our two-phase data (Table 3).

Discussion of the two-phase data

Examination of our 2 kbar data reveals an obvious break in slope along the diopside limb between 1100° and 1150°C as shown in Figure 3, which includes data from 900°–1100°C not given in Table 3. A similar, though much less obvious, break occurs between 1050° and 1100°C at 5 and 10 kbar. X-ray film patterns of the 1150°C, 2 kbar runs exhibit splitting of the 311, 112, and 202 diopside reflections. These particular reflections are noteworthy in that all show a large shift in position as a function of composition, relative to other diopside reflections. This feature (*i.e.*, splitting or broadening of these diopside reflections) is also observed in a number of runs at 5 and 10 kbar, but is always restricted to the temperature interval 1100°–1250°C. (In passing, we hasten to add that the splitting of X-ray reflections is a feature not unknown from other investigations of "simple" pyroxene systems, as noted by Bell and Davis, 1969).

To investigate the cause of this behavior, a series of compositions across the range $di_{95}en_5$–$di_{80}en_{20}$ were heated for 3 days at 1150°C and 2 kbar (Table 1). X-ray films of the products showed that the compositions $di_{95}en_5$ and $di_{92.5}en_{7.5}$ crystallized to single-phase material with no indication of peak splitting. However, for each of the compositions $di_{90}en_{10}$, $di_{87.5}en_{12.5}$, $di_{85}en_{15}$, and $di_{82.5}en_{17.5}$, the 311, 112, and 202 peaks of diopside were unquestionably split; the composition $di_{80}en_{20}$ showed only faint evidence of peak splitting. Trace amounts of orthoenstatite were present in the products corresponding to compositions more $Mg_2Si_2O_6$-rich than $di_{85}en_{15}$, which is consistent with the limit of solubility of $Mg_2Si_2O_6$ in diopside as shown in Figure 3.

A possible explanation for these results is that there exists a narrow two-phase region between the compositions $di_{92.5}en_{7.5}$ and $di_{85}en_{15}$ at 1150°C, 2 kbar. To investigate this possibility further, two samples of single-phase clinopyroxene ($di_{90}en_{10}$ and $di_{85}en_{15}$), previously synthesized at 1350°C and 1 bar, and one sample of a homogeneous glass of composition $di_{85}en_{10}q_5$ were heated (hydrothermally) for 17 hours at 1200°C and 2 kbar. X-ray films showed no evidence of unmixing (*i.e.*, peak splitting) for any of the samples. If a narrow region of two-phase unmixing does exist, then these samples would be expected to show at least incipient unmixing.

As the above results are not definitive, a series of runs were undertaken to supplement the X-ray Guinier data with electron probe microanalysis. A new set of compositions was prepared (on a mole percent basis) as mechanical mixtures of crystalline diopside and clinoenstatite. A split of each composition was heated to 1420°C at 1 bar for approximately 30 minutes and then quenched, in order to obtain a series of reference homogeneous glasses. Electron probe microanalyses (20 kV and 0.04 microamps) of the glasses were made (Table 4) using GSFC #37 diopside (Hess, 1949, p. 662, analysis no. 35: CaO, 24.90 wt percent; MgO, 17.19; SiO_2, 54.51) as a standard. From the other splits, hydrothermal crystallizations were carried out at 1150°C, 2 kbar, 3 days. Electron probe microanalyses, recast in terms of mole fraction $Mg_2Si_2O_6$ (N_{en}), are given in Table 4, together with supplemental X-ray data. No orthoenstatite crystals were encountered in the course of microanalysis, nor were any orthoenstatite reflections observed in the X-ray film patterns. The probe analyses therefore present a problem in that many are significantly more $CaMgSi_2O_6$-rich than the corresponding starting material compositions (particularly DE 10–DE 17.5). We believe that this skewing of compositions toward diopside reflects in large part the problems involved in analyzing 5–10 μ size particles by means of the electron microprobe. Only relatively large diopside crystals were analyzed, as the bulk of the sample was of a grain size too small for analysis. These large particles may be expected to undergo less chemical change in the equilibrium direction than the smaller particles, if a diffusion control is assumed. Since the starting materials were mixtures of crystalline $CaMgSi_2O_6$ and $Mg_2Si_2O_6$,

TABLE 4. Results of Electron Probe Microanalyses of Diopside Crystalline Solutions

Composition	*N_{en}(glass)	**N_{en}(crystals)	#$2\theta_{112}/N_{en}$
DE 2.5	0.028	0.046 (0.015 - 0.069)	40.742/0.016
DE 5	0.055	0.043 (0.024 - 0.060)	
DE 7.5	0.072	0.065 (0.020 - 0.132)	40.801/0.083
DE 10	0.094	0.040 (0.021 - 0.062)	
DE 12.5	0.129	0.082 (0.049 - 0.145)	°40.888/0.154
DE 15	0.153	0.047 (0.011 - 0.131)	
DE 17.5	0.170	0.040 (0.026 - 0.051)	°40.899/0.162

Electron probe microanalyses obtained by means of computer program written by Doan and Schmadebeck (1972) after the method of Bence and Albee (1968).

*GSFC No. 37 diopside (Hess, 1949, analysis No. 35: CaO, 24.90; MgO, 17.19; SiO_2, 54.51) used as standard for glass analyses. N_{en} represents average of 5 points.

**Glass DE 10 (CaO, 23.87; MgO, 20.73; SiO_2, 56.80) used as standard for crystal analyses. Range of individual analyses given in (); N_{en} represents average of 5 or more grains.

#Cu K_α radiation

°Diopside 112 reflection split: only higher 2θ peak measurable.

the analyses indicating compositions more $CaMgSi_2O_6$-rich than the respective bulk compositions are not surprising. Out of 33 individual grains analyzed for the compositions DE 7.5–DE 17.5, only five showed $N_{en} > 0.073$ and, of these, three had $N_{en} > 0.131$ (the other two were $N_{en} = 0.082$ and 0.097). Thus the electron microprobe results show some indication of a composition hiatus $0.07 < N_{en} < 0.13$ similar to that suggested by the pronounced peak splitting observed on the Guinier films.

In summary, the experimental data indicate an obvious break in the diopside limb at 2 kbar (the break is less pronounced at higher pressure). This break may be attributed either to (1) non-equilibrium in runs below 1100°C or (2) a narrow region of two-phase unmixing. Non-equilibrium, although strongly suggested by lack of reversibility of the diopside limb at 900°C, 2 kbar (Fig. 3), is difficult to accept conclusively since the orthoenstatite limb proved reversible. Results of detailed X-ray work generally support the alternative possibility of two-phase unmixing, although supplemental microprobe analyses are clearly not definitive (Table 4). Unfortunately, this alternative raises further unanswered questions with regard to possible polymorphism of diopside crystalline solutions. At present we know of no satisfactory explanation in terms of either the diopside structure or the physical chemistry of the system for the apparent inflection, or discontinuity, in the diopside limb.

Numerical Analysis of the Two-Phase Data

Preliminary statement

In our study of the binary join $CaMgSiO_4$–Mg_2SiO_4 (Warner and Luth, 1973), we derived an equation of state for monticellite-forsterite crystalline solutions through the application of a simple Margules-type solution model to experimental two-phase data for this system. The $CaMgSi_2O_6$–$Mg_2Si_2O_6$ pyroxene join differs from the olivine system in that the coexisting solvus phases need not obey the same thermodynamic equation of state. Diopside crystallizes as a monoclinic phase with $C2/c$ structure, whereas orthoenstatite exhibits orthorhombic symmetry and belongs to space group *Pbca*. This difference in the end-member structures requires a careful definition of the standard state to which the crystalline solution series is referred, since the Gibbs function is presumably not continuous across the join. In this particular system, the problem is further complicated by the fact that $CaMgSi_2O_6$ with orthoenstatite structure is unknown (Saxena, personal communication). Hence, the methods previously applied to the $CaMgSiO_4$–Mg_2SiO_4 system to obtain information on thermodynamic mixing functions for that crystalline solution series are not applicable to the system $CaMgSi_2O_6$–$Mg_2Si_2O_6$. [Instead of treating mixing parameters for the crystals as a whole, it may be preferable to consider Ca/Mg mixing in the *M*2 site and the calculation of "partial" thermodynamic functions of mixing (Saxena, personal communication).]

However, the two-phase data can be used to derive analytic expressions for the solvus boundary (Thompson and Waldbaum, 1969). An analytic representation of the data is more useful than the conventional isobaric temperature-composition section in that it affords greater ease of manipulation and may be used to interpolate or extrapolate to P, T conditions not investigated. Numerical analysis of the two-phase data may be undertaken on the basis of an empirical parametric formulation, such as the so-called *'r–s'* method of Thompson and Waldbaum (1969), or in terms of a Margules-type formulation (Thompson, 1967). For our present purposes, we have chosen to adopt the two-constant Margules equation (Thompson, 1967). We stress that in using a Margules representation, we are interested only in mathematical quantities in an analytic, curve-fitting sense, and not in assigning thermodynamic significance to them.

Treatment of data and results of numerical analysis

Since the form of the solvus boundary is demonstrably asymmetric (Fig. 3), at least two parameters are necessary for adequate representation of the two-phase data. For each observed pair of coexisting phases (Table 3), values for the Margules parameters W_{G1} and W_{G2} (Thompson, 1967) were computed (1 and 2 refer to the components $CaMgSi_2O_6$ and $Mg_2Si_2O_6$, respectively). In order to derive expressions for these parameters as simple functions of the variables P and T, the resulting sets of values were subjected to analysis by the method of least squares. Standard deviation of the dependent variable, s_y, and standard errors of the least squares coefficients, e_j, were computed from the equations (Deming, 1943):

$$s_y = \left(\sum_{i=1}^{n} (y_i(\text{obs}) - y_i(\text{calc}))^2/(n - p) \right)^{1/2} \qquad (1)$$

$$e_j = s_y |c_{jj}|^{1/2}, \quad (2)$$

where n represents the number of data points, p indicates the number of adjustable parameters in the fitted polynomial, and c_{jj} are diagonal terms of the inverse normal equations matrix.

Results of least-squares fits to W_{G1} and W_{G2} are given in Table 5. According to s_y, the best equation representing $W_{G1}(P, T)$ is of the form

$$W_{G1} = A + BT + DP \quad (3)$$

For W_{G2} (P, T), the smallest standard deviation ($s_y = 356.0$) is obtained with an equation containing a T^2 term and a PT cross-term. However, the standard errors of the coefficients exceed the values of the coefficients themselves for both pressure-dependent terms in this equation. In fact, coefficients for all pressure-dependent terms in all fits to W_{G2} (P, T) are not statistically meaningful, and we therefore conclude that W_{G2} is pressure independent. On the basis of significant improvement in s_y, the retention of a T^2 term would seem justifiable. Temperature-composition diagrams calculated using a quadratic equation for W_{G2} (see following section) yield physically improbable results when extrapolated to temperatures both above and below the range of experimental data (1100°–1300°C). On the other hand, a simple, linear T dependence provides a wholly satisfactory representation over the range 1100°–1300°C and also proves versatile as an extrapolation function. We therefore conclude that the most appropriate representation for W_{G2} (P, T) is obtained with an equation of the form

$$W_{G2} = A + BT \quad (4)$$

TABLE 5. Results of Least Squares Fits to W_{G1} (P,T) and W_{G2} (P,T)

A	B	C	D	E	F	s_y
			a) $W_{G1}(P,T)$			
12,763 ±991	-2,666 ±674					238.9
33,535 ±21,984	-30,901 ±29,859	9,578 ±10,126				239.4
8,605 ±85			41.9 ±12.8			252.7
	5,752 ±126		64.4 ±27.8			555.9
12,189 ±864	-2,419 ±581		36.6 ±10.4			204.5
10,512 ±2,168	-1,282 ±1,467		268.6 ±274.9	-157.5 ±186.5		205.5
2,199 ±21,268	9,975 ±28,685	-3,809 ±9,694	273.5 ±279.3	-159.5 ±189.3		208.6
43,866 ±47,430	-46,337 ±64,075	15,194 ±21,629	-5,976 ±6,364	8,295 ±8,603	-2,855 ±2,904	208.7
			b) $W_{G2}(P,T)$			
24,032 ±1,697	-12,215 ±1,153					408.9
-79,986 ±33,112	129,180 ±44,974	-47,963 ±15,252				360.5
5,918 ±295			27.9 ±44.2			873.3
	3,889 ±250		56.1 ±55.1			1,099.6
24,011 ±1,756	-12,206 ±1,181		1.3 ±21.2			415.7
26,639 ±4,428	-13,987 ±2,996		-362.1 ±561.5	246.7 ±380.9		419.8
-100,110 ±36,300	157,650 ±48,959	-58,081 ±16,545	-286.7 ±476.6	215.2 ±323.1		356.0
-163,620 ±81,246	243,490 ±109,760	-87,047 ±37,050	9,240 ±10,901	-12,671 ±14,736	4,351 ±4,974	357.5

s_y = estimated standard error of dependent variable

$W_G = A + B(T/1000) + C(T/1000)^2 + DP + EP(T/1000) + FP(T/1000)^2$

units: T, °K; P, kbar; W_G, cal/mole

1 : $CaMgSi_2O_6$ 2 : $Mg_2Si_2O_6$

Calculated temperature-composition diagrams

The equations W_{G1} (P,T) and W_{G2} (P,T) may be resolved by iterative techniques to obtain values for N_{2A} and N_{2B} at any desired pressure and temperature (Thompson and Waldbaum, 1969). A more direct method of computing values for N_{2A} and N_{2B} involves formulation of an explicit expression for the activity function in terms of W_{G1} and W_{G2} (*i.e.*, Thompson, 1967, p. 349) and utilizes the condition of equivalence of chemical potentials for the isobaric-isothermal coexistence of the two phases as defined in terms of relative activities (Scatchard, 1940; Luth and Fenn, 1973). (Although activity-composition relations for the system $CaMgSi_2O_6$–$Mg_2Si_2O_6$ are poorly defined because of differences in crystal structure between the end-member phases, the use here of the activity function to compute N_{2A} and N_{2B} is strictly numerical and implies no thermodynamic validity to the quantities employed.)

In Figure 3 an isobaric temperature-composition section (solid curves) calculated at 2 kbar (procedure described in Luth and Fenn, 1973) is shown for comparison with the experimental two-phase data. The appearance of a stability field for "iron-free" pigeonite on the join $CaMgSi_2O_6$–$MgSi_2O_6$ (Kushiro, 1969, 1972; Kushiro and Yoder, 1970; Warner, 1971; Yang and Foster, 1972) provides an upper stability limit for the diopside-orthoenstatite two-phase coexistence. Although not indicated in Figure 3, this upper limit is probably reached at a

temperature near 1330°C at 2 kbar, well below the calculated critical temperature of 1525°C.

The analytic expressions for W_{G1} and W_{G2} permit extrapolation of the solvus boundary to higher pressures. In Figure 4 the solvus calculated for $P = 30$ kbar is compared with the 30 kbar solvus determined experimentally by Davis and Boyd (1966). The agreement between the two solvi is quite good : between 900° and 1425°C the maximum discrepancy between the calculated and observed solvus on the diopside side is about 0.03 N_{en}. Our calculated orthoenstatite limb below 1400°C is several mole percent more $Mg_2Si_2O_6$-rich than that reported by Davis and Boyd (1966). However, more recent data obtained by means of electron probe microanalysis indicate that their original determinations of the maximum solubility of $CaMgSi_2O_6$ in orthoenstatite are consistently several mole percent too $Mg_2Si_2O_6$-poor (Boyd, personal communication).

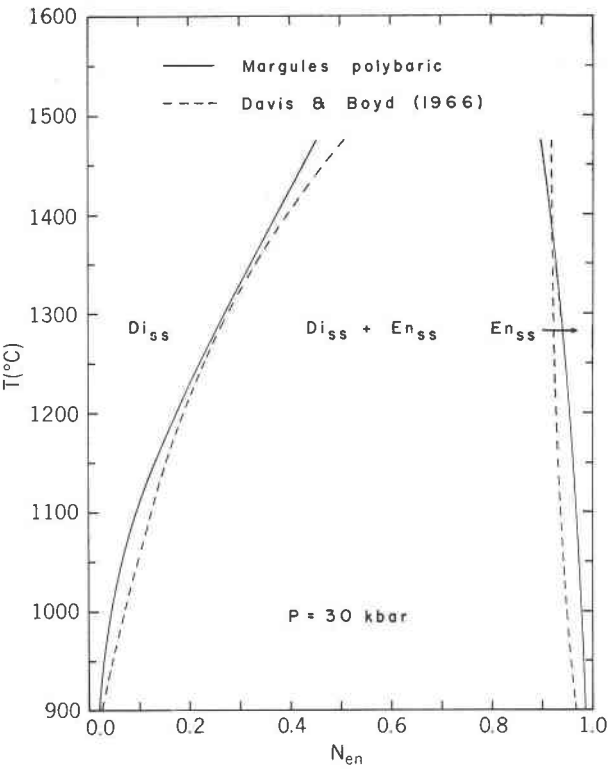

FIG. 4. Comparison of calculated and observed solvus boundaries of the diopside-orthoenstatite two-phase region at 30 kbar. Calculated boundary (solid curve) obtained from extrapolation to 30 kbar of polybaric expressions for W_{G1} and W_{G2}. Dashed curve represents solvus boundary determined by Davis and Boyd (1966) at 30 kbar.

Petrologic Application

Various aspects of the chemistry and mineralogy of pyroxenes have been used to estimate physical conditions of crystallization or equilibration of natural pyroxene-bearing mineral assemblages. The coexistence of the two phases, clinopyroxene and orthopyroxene, is characteristic of many mafic and ultramafic rocks, and the Ca distribution between these two phases potentially provides a useful geothermometer. The variation in Ca content of orthopyroxene saturated with clinopyroxene is much less sensitive to temperature than is the variation in Ca content of clinopyroxene saturated with orthopyroxene; for this reason, the latter is a more useful parameter.

Application of the results from the join $CaMgSi_2O_6$–$Mg_2Si_2O_6$ to natural occurrences involves several inherent assumptions and limitations. One assumption is that the composition of diopside coexisting with orthoenstatite is, for any given temperature, largely pressure insensitive (*e.g.*, Davis and Boyd, 1966). The experimental data obtained in the present study indicate that this assumption is a fairly good one. Within the limits of statistical uncertainty, W_{G2} was found to be independent of pressure. As a result, the position of the diopside limb of the solvus changes little as a function of pressure. For example, using equations (3) and (4) for W_{G1} and W_{G2}, the composition of diopside coexisting with orthoenstatite at 1200°C is computed to be $N_{en} = 0.201$ at 2 kbar and $N_{en} = 0.177$ at 30 kbar, which is a difference only slightly greater than the uncertainty in the solvus boundary.

A second assumption is that presence of other components in minor amounts does not significantly modify the diopside-orthenstatite solvus boundary. Recent experimental data outlining the extent of pyroxene crystalline solution in the system $CaSiO_3$–$MgSiO_3$–Al_2O_3 at 1200°C and 30 kbar (Boyd, 1970a; 1970b) suggest that the results for the join $CaMgSi_2O_6$–$Mg_2Si_2O_6$ may be reasonably applied to pyroxenes containing up to 3 to 4 wt percent Al_2O_3. Experimental data pertaining to the effect of other components are notably lacking. In a qualitative sense, the trend lines for pyroxenes crystallizing from layered intrusives imply that the solvus shrinks rapidly with enrichment in $FeSiO_3$. Thus application of the results for the iron-free system to pyroxenes containing more than a few wt percent $FeSiO_3$ is hazardous.

The third, and most important assumption, is that the temperatures obtained have any real petrologic

significance. To verify this, careful petrographic study is required to demonstrate that subsequent events during the cooling history of a particular two-pyroxene assemblage, for example, unmixing of the pyroxene phases, have not obscured the metamorphic or igneous episode under consideration.

Figure 5 summarizes the results from this study on a *P-T* grid. Plotted in this figure are isocompositional curves indicating maximum solubility of $Mg_2Si_2O_6$ in diopside (in mole percent). These curves are based on the least-squares equations W_{G1} (P,T) and W_{G2} (P,T) (polynomial coefficients given in Table 5). Also shown in Figure 5 are the *P–T* curves outlining the lower stability limit of pigeonite on the $CaMgSi_2O_6$–$Mg_2Si_2O_6$ join (from Kushiro and Yoder, 1970, Fig. 18) and the reaction En_{ss} = Di_{ss} + Pr_{ss}, for which there is little experimental control (Warner, 1971).

Using Figure 5, temperatures of equilibration or crystallization for natural two-pyroxene assemblages may be estimated by simply measuring the molar Ca/(Ca + Mg) ratio of diopsidic clinopyroxene coexisting with enstatitic orthopyroxene. Analyses of diopside inclusions from peridotite nodules in kimberlites show that compositions of these pyroxenes lie near the binary join $CaMgSi_2O_6$–$Mg_2Si_2O_6$ (Davis and Boyd, 1966; Boyd, 1969) and hence are amenable to consideration in terms of Figure 5. The available analyses show a bimodal distribution for the molar Ca/(Ca + Mg) ratios, with a lack of intermediate compositions (Boyd, 1969, 1970b). (This may be an effect of sampling, as more recent analyses (Boyd, 1972) indicate that there are some intermediate diopsides.) Consequently, two distinct populations are obtained in terms of estimated equilibration temperatures. The cluster of calcic diopsides (Boyd, 1970b) yield equilibration temperatures near 1025°C (range 900°-1125°C), while the subcalcic diopsides appear to have formed between 1325°C and 1400°C.

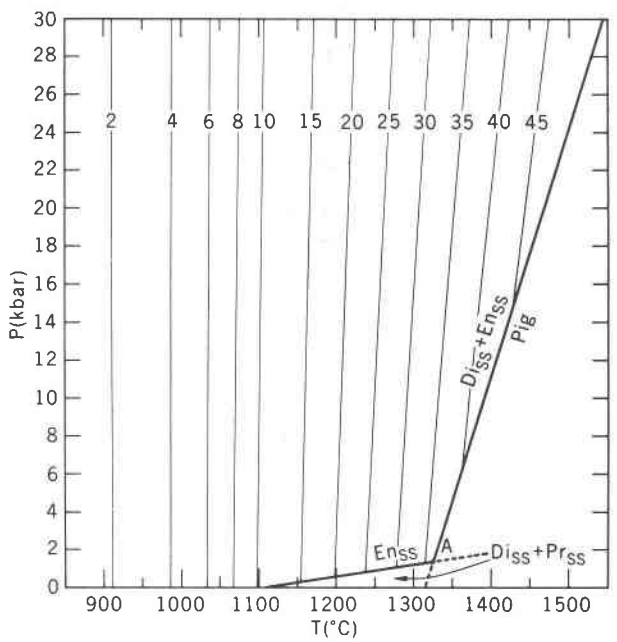

FIG. 5. Maximum solubility of $Mg_2Si_2O_6$ in Di_{ss} (in mole percent) as a function of pressure and temperature. Also shown are curves representing the lower stability limit of pigeonite on the $CaMgSi_2O_6$–$Mg_2Si_2O_6$ join (Kushiro and Yoder, 1970, Fig. 18) and the low pressure breakdown of En_{ss} to Di_{ss} and Pr_{ss}. The intersection of these curves (at A, position uncertain) is an invariant point in the binary system. Abbreviations: Di_{ss}, diopside solid solution; En_{ss}, orthoenstatite solid solution; Pr_{ss}, protoenstatite solid solution; Pig, pigeonite.

In summary, the experimental results for the diopside-orthoenstatite two-phase region may be applied to natural pyroxenes whose compositions permit approximation as phases in the system $CaMgSi_2O_6$–$Mg_2Si_2O_6$. The polybaric Margules representation of the two-phase region verifies that the diopside solvus boundary is largely pressure insensitive. An advantage of the polybaric formulation is that the pressure dependence may be quantified (Fig. 5); this may improve the estimated equilibration temperatures for specific applications.

Acknowledgments

This paper is based on a Ph.D. dissertation by R. D. Warner accepted by the Department of Geology, Stanford University. The financial support of the National Science Foundation, both in the way of a graduate fellowship (RDW) and through NSF Grant GA 4164 (WCL) is most gratefully acknowledged. Additional experimental data was collected by Warner while on a Resident Research Associateship in the Planetology Branch at Goddard Space Flight Center, for which program financial assistance was kindly provided by the National Academy of Sciences. We wish to thank Mr. P. R. Gordon, for his technical assistance in operating the high pressure apparatus, Mr. Frank Wood, for performing electron probe microanalyses, Dr. P. M. Fenn, for helping to develop the computer programs used in the numerical analysis, and Dr. S. K. Saxena, for contributions he has advanced through numerous discussions.

References

ATLAS, L. (1952) The polymorphism of $MgSiO_3$ and solid-state equilibria in the system $MgSiO_3$–$CaMgSi_2O_6$. *J. Geol.* **60**, 125–147.

BELL, P. M., AND B. T. C. DAVIS (1969) Melting relations

in the system jadeite-diopside at 30 and 40 kilobars. *Am. J. Sci.* **267-A,** 17–32.

BENCE, A. E., AND A. L. ALBEE (1968) Empirical correction factors for the electron microanalysis of silicates and oxides. *J. Geol.* **76,** 382–403.

BOYD, F. R. (1969) Electron-probe study of diopside inclusions from kimberlite. *Am. J. Sci.* **267-A,** 50–69.

——— (1970a) The system $CaSiO_3$–$MgSiO_3$–Al_2O_3. *Carnegie Inst. Wash. Year Book,* **68,** 214–221.

——— (1970b) Garnet peridotites and the system $CaSiO_3$–$MgSiO_3$–Al_2O_3. *Mineral. Soc. Am. Spec. Pap.* **3,** 63–75.

———, AND P. H. NIXON (1972) Ultramafic nodules from the Thaba Putsoa kimberlite pipe. *Carnegie Inst. Wash. Year Book,* **71,** 362–373.

———, AND J. F. SCHAIRER (1964) The system $MgSiO_3$–$CaMgSi_2O_6$. *J. Petrology,* **5,** 275–309.

———, ———, AND B. T. C. DAVIS (1964) Effects of pressure on the melting and polymorphism of enstatite, $MgSiO_3$. *J. Geophys. Res.* **69,** 2101–2109.

DAVIS, B. T. C., AND F. R. BOYD (1966) The join $Mg_2Si_2O_6$–$CaMgSi_2O_6$ at 30 kilobars pressure and its application to pyroxenes from kimberlites. *J. Geophys. Res.* **71,** 3567–3576.

DEMING, W. E. (1943) *Statistical Adjustment of Data.* John Wiley and Sons, New York, 261 pp.

DOAN, A. S., JR., AND R. L. SCHMADEBECK (1972) A new concise treatment of X-ray microprobe data after Bence and Albee. *Goddard Space Flight Center Computer Library, Probe-M,* **00124.**

EVANS, H. T., D. E. APPLEMAN, AND D. S. HANDWERKER (1963) The least square refinement of crystal unit cells with powder diffraction data by an automatic computer indexing method. *Progr. Annu. Meet. Am. Crystallogr. Assoc.,* 42–43.

HESS, H. H. (1949) Chemical composition and optical properties of common clinopyroxenes. Part I. *Am. Mineral.* **34,** 621–666.

KUSHIRO, I. (1969) The system forsterite-diopside-silica with and without water at high pressures. *Am. J. Sci.* **267-A,** 269–294.

——— (1972) Determinations of liquidus relations in synthetic silicate systems with electron probe analysis: The system forsterite-diopside-silica at 1 atmosphere. *Am. Mineral.* **57,** 1260–1271.

———, AND J. F. SCHAIRER (1963) New data on the system diopside-forsterite-silica. *Carneigie Inst. Wash. Year Book,* **62,** 95–103.

———, AND H. S. YODER, JR. (1970) Stability field of iron-free pigeonite in the system $MgSiO_3$–$CaMgSi_2O_6$. *Carnegie Inst. Wash. Year Book,* **68,** 226–229.

———, ———, AND M. NISHIKAWA (1968) Effect of water on the melting of enstatite. *Geol. Soc. Am. Bull.* **79,** 1685–1692.

LUTH, W. C., AND P. M. FENN (1973) Calculation of binary solvi with special reference to the sanidine-high albite solvus. *Am. Mineral.* **58,** 1009–1015.

SCATCHARD, G. (1940) The calculation of the composition of phases in equilibrium. *Am. Chem. Soc.* **62,** 2426–2429.

SMITH, J. V. (1969) Crystal structure and stability of the $MgSiO_3$ polymorphs: physical properties and phase relations of Mg, Fe pyroxenes. *Mineral. Soc. Am. Spec. Pap.* **2,** 3–29.

THOMPSON, J. B., JR. (1967) Thermodynamic properties of simple solutions, In *Researches in Geochemistry,* Vol. 2, Ed. P. H. Abelson. John Wiley and Sons, New York, pp. 340–361.

———, AND D. R. WALDBAUM (1969) Analysis of the two-phase region halite-sylvite in the system NaCl-KCl. *Geochim. Cosmochim. Acta,* **33,** 671–690.

WARNER, R. D. (1971) *Experimental investigations in the system CaO-MgO-SiO_2-H_2O.* Ph.D. Thesis, Stanford University, 165 pp.

———, AND W. C. LUTH (1973) Two-phase data for the join monticellite ($CaMgSiO_4$)-forsterite (Mg_2SiO_4): Experimental results and numerical analysis. *Am. Mineral.* **58,** 998–1008.

YANG, HOUNG-YI, AND W. R. FOSTER (1972) Stability of iron-free pigeonite at atmospheric pressure. *Am. Mineral.* **57,** 1232–1241.

Manuscript received, July 2, 1973; accepted for publication, September 7, 1973.